Irradiance Forecasting for the Power Prediction of Grid-Connected Photovoltaic Systems

Elke Lorenz, Johannes Hurka, Detlev Heinemann, and Hans Georg Beyer

***Abstract*—The contribution of power production by photovoltaic (PV) systems to the electricity supply is constantly increasing. An efficient use of the fluctuating solar power production will highly benefit from forecast information on the expected power production. This forecast information is necessary for the management of the electricity grids and for solar energy trading. This paper presents an approach to predict regional PV power output based on forecasts up to three days ahead provided by the European Centre for Medium-Range Weather Forecasts (ECMWF). Focus of the paper is the description and evaluation of the approach of irradiance forecasting, which is the basis for PV power prediction. One day-ahead irradiance forecasts for single stations in Germany show a *rRMSE* of 36%. For regional forecasts, forecast accuracy is increasing in dependency on the size of the region. For the complete area of Germany, the *rRMSE* amounts to 13%. Besides the forecast accuracy, also the specification of the forecast uncertainty is an important issue for an effective application. We present and evaluate an approach to derive weather specific prediction intervals for irradiance forecasts. The accuracy of PV power prediction is investigated in a case study.**

***Index Terms*—Forecasting, photovoltaic power systems, power generation meteorological factors, solar radiation.**

I. Introduction

DUE to the strong increase of renewable energies, the significance of the prediction of meteorological quantities, such as wind speed and solar irradiance, is rising.

Today, wind power prediction systems have already shown their strong economic impact and improve the integration of wind energy into the electricity grid (see, e.g., [1]). Accordingly, the prediction of solar yields will become more and more important for utilities, which have to integrate increasing amounts of solar power, especially for countries where legislation encourages the deployment of solar power plants. The Spanish feed-in law already includes incentives for correct predictions of solar yields for the next day. In Germany, the installed photovoltaic (PV) power amounts to more than 5 GW. In Bavaria, where a large number of these PV systems is installed, the share of solar power injected on power grids can reach around 10% during peak hours on sunny days.

Manuscript received September 08, 2008; revised December 22, 2008. Current version published April 29, 2009. This work was supported in part by the virtual Institute of Energy Meteorology (vIEM) of the German Helmholtz Association.

E. Lorenz, J. Hurka, and D. Heinemann are with the University of Oldenburg, Institute of Physics, Energy and Semiconductor Research Laboratory, Energy Meteorology Group, 26111 Oldenburg, Germany (e-mail: elke.lorenz@uni-oldenburg.de; johannes.hurka@uni-oldenburg.de; detlev.heinemann@uni-oldenburg.de).

H. G. Beyer is with the University of Applied Sciences Magdeburg-Stendal, Institute of Electrical Engineering, Breitscheidstr.2 D-39114, Magdeburg, Germany (e-mail: hans-georg.beyer@hs-magdeburg.de).

Digital Object Identifier 10.1109/JSTARS.2009.2020300

Forecast information on the expected solar and wind power production is necessary for the management of electricity grids, for scheduling of conventional power plants and also for decision making on the energy market, as described in detail, e.g., in [2]. Reference [3] demonstrates the benefit of wind power predictions for energy trading.

An overview on different approaches to forecast solar irradiance is given in [4]. Depending on the application and the corresponding time scale different approaches for forecasting may be appropriate. For very short-term forecasting in a temporal range up to some hours, we have proposed an approach based on the analysis of satellite data [4]. For utility applications, forecasts up to two days ahead or even beyond are required. This is the time range where the output from numerical weather prediction (NWM) models is applied. Irradiance forecasts based on the mesoscale NWP model MM5 (see [5]) have been evaluated, e.g., in [6]–[8]. Reference [9] presents an approach to improve solar radiation forecasts of the ETA model of the National Centers of Environmental Prediction (NCEP) by application of Neural Networks. A solar radiation forecasting model based on the U.S. National Forecast Data Base was developed by [10], and [11] has investigated different approaches of irradiance forecasting with special focus on the influence of aerosols.

Here, we present a forecasting scheme to derive predictions of PV power output based on forecasts up to three days ahead provided by the European Centre for Medium-Range Weather Forecasts (ECMWF). The global model run by the ECMWF provides forecasts of solar irradiance and cloud parameters with a temporal resolution of 3 h and a spatial resolution of $0.25^\circ \times 0.25^\circ$. For the management of electricity grids, forecasts of the expected solar power input are necessary on an hourly basis. In order to derive optimized, site-specific, hourly forecasts, we have investigated different approaches.

For the utility companies, a forecast of the ensemble production of all PV systems contributing to a control area is necessary. Hence, the forecast accuracy is evaluated not only for single systems but also for ensembles of PV systems.

For an effective application of the power forecast, information on the forecast accuracy is an important issue. The benefit of prediction intervals for power forecasts is discussed, e.g., in [12] and [13]. The forecast uncertainty depends on the meteorological situation: Situations with inhomogeneous clouds generally are more difficult to forecast and show a lower accuracy than forecasts for clear sky days. We introduce a method to calculate situation-specific prediction intervals for single sites based on a detailed accuracy assessment for irradiance forecasts. Furthermore, we propose a procedure to derive prediction intervals also for arbitrary ensembles of stations.

1939-1404/$25.00 © 2009 IEEE

Authorized licensed use limited to: Electricity Generating Authority of Thailand. Downloaded on August 23,2021 at 06:27:58 UTC from IEEE Xplore. Restrictions apply.

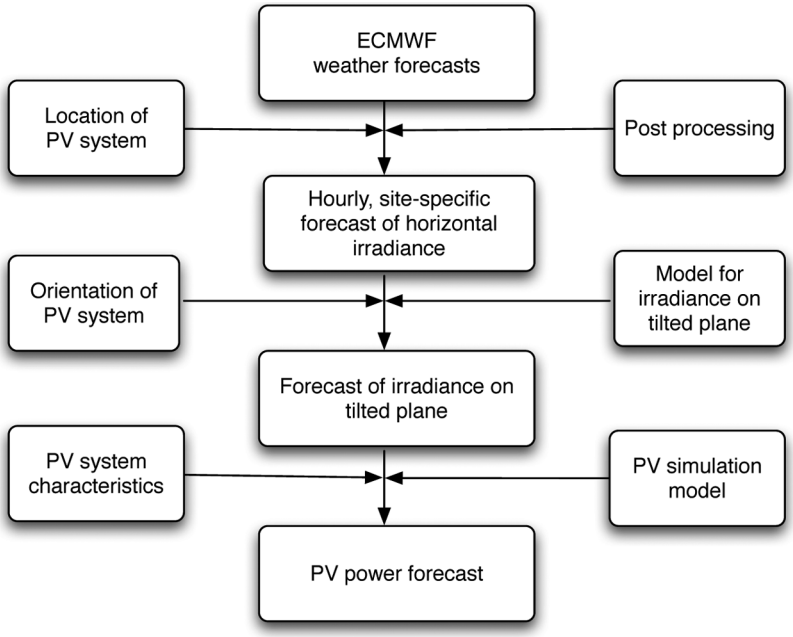

Fig. 1. Overview on forecasting scheme.

The performance of the complete chain of power prediction is analyzed in a case-study for a small ensemble of PV systems in Southern Germany.

II. Overview on Forecasting Scheme

The prediction of the PV power production is based on irradiance forecasts up to three days ahead provided by the global model of the ECMWF. Fig. 1 illustrates the different steps to derive a forecast of PV power production from ECMWF irradiance forecasts. For each step the used models and necessary additional information on the PV system are specified. In a first step, site-specific hourly forecasts are derived from the low-resolution ECWMF forecasts. In a second step, the forecast of the global horizontal irradiance has to be converted to the module plane with a tilted irradiance model. Finally, the power output forecast is obtained by applying a PV simulation model to the forecasted irradiances.

III. Ground Measurement Data

A. Irradiance Data

For the investigation, we used measured irradiance data of more than 200 meteorological stations in Germany. The distribution of these stations in Germany is shown in Fig. 2.

The evaluation was performed for the period from 1.1.2007 to 31.10.2007.

B. Measurement of Power Output

PV power forecasts were evaluated in a case study for an ensemble of 11 PV systems distributed over an area of 200 km $\times$ 120 km in Southern Germany. Their locations are shown in Fig. 2. The measured data were available with hourly resolution.

The evaluation was performed for April and July 2006. These two months with different meteorological conditions were chosen in order to investigate the influence of weather conditions on the forecast accuracy.

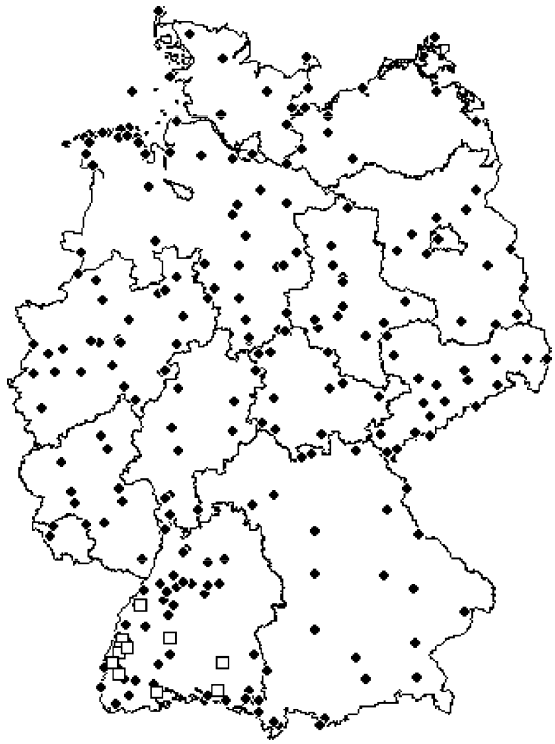

Fig. 2. Distribution of the meteorological stations with irradiance measurements (dark dots) and the PV sites (light squares).

IV. Measures of Accuracy

In general, for performance evaluation of a forecast a lot of different issues have to be taken into account. A comprehensive overview on different aspects of forecast verification is given in [14].

Authorized licensed use limited to: Electricity Generating Authority of Thailand. Downloaded on August 23,2021 at 06:27:58 UTC from IEEE Xplore. Restrictions apply.

In this paper, we focus on few measures of accuracy that are considered to be most relevant for the intended application of power prediction. Following common practice for the evaluation of wind power predictions (e.g., [2] and [12]), we use the root mean square error

$$\mathrm{RMSE} = \sqrt{\frac{1}{N}\sum_{i=1}^{N}(x_{\mathrm{forecast,i}} - x_{\mathrm{measured,i}})^2} \qquad (1)$$

as a main score. N is the number of data pairs evaluated. The variable x represents global irradiance I_{glob}, or normalized power output $P_{\mathrm{AC}}/P_{\mathrm{nom}}$, respectively. The normalization of the alternating current (AC) power output P_{AC} to the nominal power P_{nom} of the PV system allows for a better comparison of different PV systems.

As additional scores, we use the mean value of the errors

$$\mathrm{BIAS} = \frac{1}{N}\sum_{i=1}^{N}(x_{\mathrm{forecast,i}} - x_{\mathrm{measured,i}}) \qquad (2)$$

and the standard deviation of errors

$$\mathrm{STDERR} = \sqrt{\frac{1}{N}\sum_{i=1}^{N}(x_{\mathrm{forecast,i}} - x_{\mathrm{measured,i}} - \mathrm{BIAS})^2}. \qquad (3)$$

These accuracy measures are related to each other by

$$\mathrm{RMSE}^2 = \mathrm{BIAS}^2 + \mathrm{STDERR}^2. \qquad (4)$$

The accuracy measures are calculated for hourly values. Only hours with daylight ($I_{\mathrm{glob,i}} > 0$) are considered for the calculation of BIAS and RMSE, night values with no irradiance are excluded from the evaluation.

Also relative values of the error measures (*rRMSE*, *rBIAS*) will be given in the following sections. Normalization is done with respect to mean ground measured irradiance of the considered period.

V. Irradiance Forecast

A. Method

We propose a forecasting approach based on irradiance forecasts of the ECMWF. In [15], a description of physical process of the implementation of the ECMWF model during the evaluation period is given. Details on the radiation transfer parameterization are described in [16].

The global model run by the ECMWF provides forecasts of solar irradiance with a temporal resolution of 3 h and a spatial resolution of $0.25^\circ \times 0.25^\circ$. For the management of electricity grids, forecasts of the expected solar power input are necessary on an hourly basis. In order to derive site-specific hourly forecasts, we have analyzed different approaches to refine the ECMWF global model irradiance forecasts, based on previous investigations by [6]. This analysis was performed for predictions up to 72 h.

1) Spatial Averaging and Temporal Interpolation: In [6], different spatial interpolation techniques have been investigated to optimize the forecast for a given site. The use of the arithmetic average of surrounding pixels is proposed, as the use of distance dependent weights does not improve the results. An analysis of the forecast accuracy in dependence on the number of grid points used for averaging revealed that with average values of 4 $\times$ 4 grid points best results are achieved. This corresponds to a region of approx. 100 km $\times$ 100 km for Germany. The benefit of the spatial averaging can be partly explained looking at the scaling aspect of linear regression schemes (see, e.g., [2] and [14]). The RMSE of a forecast is improved by scaling the amplitude of the prediction in accordance with the correlation of predicted and measured time series, which is one effect of the averaging procedure.

For the temporal interpolation, we consider two different approaches. A very simple approach to derive hourly resolved forecasts is the linear interpolation of the three-hourly mean values that are provided by the ECMWF (version V1).

As a second approach, we combine the forecast data with a clear sky model to better account for the typical diurnal course of irradiance. For the calculation of the clear sky irradiance we apply the model proposed by [17]. This model uses the Linke turbidity factor as a measure of the optical thickness of the atmosphere. The mean annual variation of the turbidity is described by the model of [18]. A map specifying the necessary parameters for Europe was developed in the EU-funded Satel-Light project [19].

The interpolation is performed for the clear sky index kt^*, defined as ratio of the global irradiance I_{glob} to the expected irradiance for clear sky conditions I_{clearsky}. This parameter characterizes the transmission of the irradiance through the atmosphere and is independent of the deterministic course of irradiance (see also [6]). In a first step, three-hourly mean values of $kt^*_{3h} = I_{\mathrm{glob,forec,3h}}/I_{\mathrm{clearsky,3h}}$ are calculated from the forecasted values $I_{\mathrm{glob,forec,3h}}$. In a second step, hourly values of kt^* are derived by linear interpolation, and finally the hourly resolved irradiance values are obtained as $I_{\mathrm{glob,forec}} = kt^* I_{\mathrm{clearsky}}$ (version V2).

A comparison of the two approaches for predicted clear sky situations is given in Fig. 3. The *rBIAS* and the *rRMSE* are displayed over the forecast parameter total cloud cover tcc for low values of $tcc < 0.1$ for the two approaches. The given values of tcc are derived from three-hourly model output by linear temporal interpolation and as spatial average of 4 $\times$ 4 grid points. The figure shows that for clear sky situations a significant improvement is achieved using version V2. Overall, the *rRMSE* is reduced from 17% to 12% for all situations with $tcc < 0.1$. For both approaches an underestimation of the measured irradiance is found.

2) Improved Clear Sky Forecasts: The quality of the irradiance forecast for correctly predicted clear sky situations is strongly dependent on the atmospheric input to the model. The ECMWF model considers aerosols using a worldwide climatology of the annual cycle of different aerosol types [15].

In order to investigate the potential for a better modeling of clear sky irradiances, we compare the interpolated ECWMF irradiance forecasts with the clear sky model by [17] in these situations. The forecast error when assuming I_{clearsky} as forecast value is plotted over the forecast of the total cloud cover tcc in Fig. 3 in comparison to the ECMWF based forecasts. The figure shows that for very low values of the total cloud cover

Authorized licensed use limited to: Electricity Generating Authority of Thailand. Downloaded on August 23,2021 at 06:27:58 UTC from IEEE Xplore. Restrictions apply.

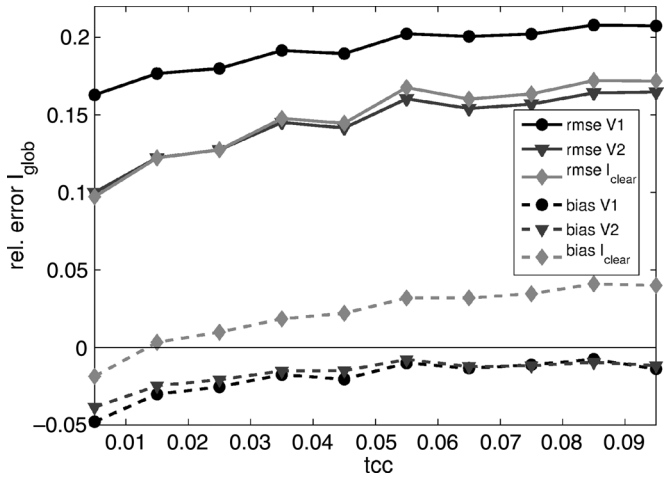

Fig. 3. Forecast errors for global irradiance over forecast of total cloud cover tcc for different approaches of forecasting (V1: linear interpolation of I_{glob}, V2: linear interpolation of kt^*, I_{clear}: Clear sky irradiance I_{clear} derived with a clear sky model is assumed as forecast value). Solid lines represent the *rRMSE* and dashed lines show the *rBIAS*.

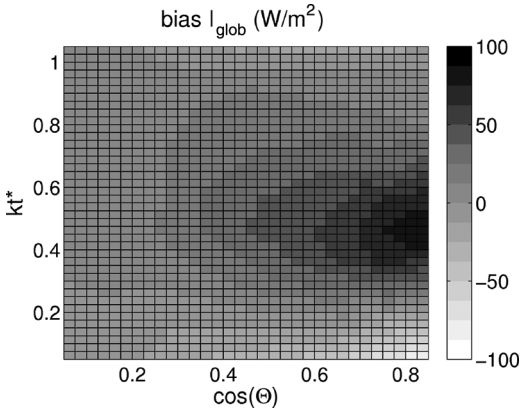

Fig. 4. BIAS of forecast of global irradiance I_{glob} with version V2+ in dependence on the cosine of the solar zenith angle $cos\Theta$ and the clear sky index kt^*.

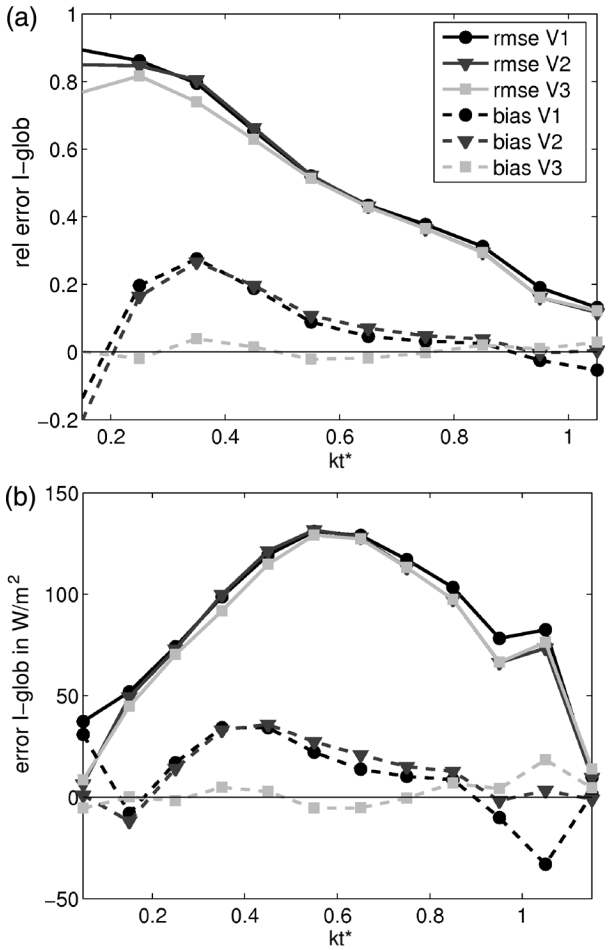

Fig. 5. Forecast errors for hourly global irradiance I_{glob} over clear sky index kt^* for the different forecasting approaches. (V1: linear interpolation of I_{glob}, V2: linear interpolation of kt^*, V3: linear interpolation of kt^* with clear sky model for clear sky situations and bias correction). Solid lines represent the RMSE and dashed lines show the BIAS. (a) Relative values *rRMSE* and *rBIAS*, normalized to the ground irradiance of the respective kt^* class. (b) Absolute values of RMSE and BIAS.

$(tcc < 0.03)$ the BIAS is smaller for the clear sky model than for the forecasts. With increasing values of tcc also partly cloudy situations are considered. Therefore, the assumption of clear sky leads to overestimation of the irradiance. According to Fig. 3 we choose $tcc = 0.03$ as threshold value. For $tcc < 0.03$ the predicted values are replaced by I_{clearsky} (Version V2+), which is suitable for the application of irradiance forecasts in the region of Germany.

3) Post Processing With Ground Data: In a last step to derive an optimized forecast of hourly values of the global irradiance, we investigate the application of a post processing procedure to correct for systematic deviations. For that purpose, we analyze the BIAS of the forecast in dependence on the cloud situation and the solar zenith angle.

Fig. 4, where the BIAS of the forecast with version V2+ is displayed over the predicted clear sky index kt^* and the cosine of the solar zenith angle $cos\Theta$, shows that there is a considerable overestimation of the irradiance for cloudy situations with clear sky index values between $kt^* = 0.3$ and $kt^* = 0.8$.

Also, [16] has observed this overestimation of the irradiance for cloudy situations and relates it to the "handling of the amount of condensed water in clouds, with too small optical thickness." For situations predicted as overcast $(kt^* < 0.2)$ the actual measured irradiance is underestimated

In order to avoid these systematic deviations, we introduce a situation specific bias correction. To allow for independent testing of this adaptation to ground data, the data were divided into training and test data. The first 15 days of each month were chosen as training set, the remaining data form the test set.

In a first step, the BIAS is modeled by a polynomial function of fourth order in the variables kt^* and $cos\Theta$. Choosing this model, a good agreement between modeled and measured BIAS is achieved. The fit parameters were derived on the training data set. The final version of the forecast (version V3) is obtained by subtracting the modeled bias $(kt^*, cos\Theta)$ from the forecast values obtained with version V2+.

Fig. 5 shows the RMSE and the BIAS over the predicted clear sky index kt^* for the different versions to forecast I_{glob} for the test data set. Fig. 5(a) shows relative values of the error measures, Fig. 5(b) gives the absolute values. For situations with no or few clouds predicted, the combination with a clear sky model (V2) improves forecast quality compared to simple linear

Authorized licensed use limited to: Electricity Generating Authority of Thailand. Downloaded on August 23,2021 at 06:27:58 UTC from IEEE Xplore. Restrictions apply.

interpolation (V1). For cloudy situations, the systematic overestimation of the irradiance is adjusted with the situations specific bias correction (V3) also on the test set. The forecast quality is high for situations predicted as clear sky ($\mathrm{kt}^* \approx 1$) with an *rRMSE* of less than 15%. Though relative forecast errors are large for overcast situations with low irradiance ($kt^* < 0.2$), the absolute RMSE values are small in these situations. Largest deviations between measurements and forecasts are found for situations with variable cloud cover, which occur mainly for $0.4 < kt^* < 0.8$.

This is illustrated also in Fig. 9(a), where time series of predicted irradiance and measured irradiance are given for six days in May 2007. The figure shows a good agreement between forecasts and measurements for clear sky days. For cloudy days, significant deviations between forecasts and measurements may occur. The hourly variation of the irradiance for days with variable clouds is not correctly modeled by the forecast.

B. Forecast Evaluation

An overall evaluation of the forecast accuracy for the different approaches in dependence on the forecast horizon is given in Fig. 6. The results are grouped according to the forecast day. Results for the first forecast day integrate forecast horizons up to 24 h, the second forecast day integrates forecast horizons from 25 to 48 h, and the third day includes forecast horizons from 49 to 72 h. The evaluation was performed on the test data set. Fig. 6(a) shows the results for a single station, while in Fig. 6(b), the mean irradiance of all stations was evaluated.

With approach V3 best results are achieved. While for single sites the differences between the three approaches are only small, for regional forecasts, a significant improvement is achieved by correction of systematic deviations.

For single sites, the *rRMSE* using approach V3 is 36.9% for the first forecast day, and increases to 46.3% for the third forecast day. For the third forecast day the application of the bias correction, which was derived for the first forecast day, leads to a negative BIAS. This could be improved by deriving a separate correction function for each forecast day.

Due to spatial averaging effects, the forecast for an ensemble of distributed stations shows much higher accuracy than the forecast for single systems. The *rRMSE* for the ensemble of all stations amounts to 13.4% for the first forecast day using approach V3, for the third forecast day, the *rRMSE* increases to 22.5%. An example time series of measured and predicted mean irradiance of all stations is given in Fig. 9(b). Spatial averaging effects cause a smoother course of the curve of power production than for single systems and the deviations between forecast and measurement are smaller.

All following results are derived on the test data set for the one day ahead forecasts using approach V3.

C. Estimation of Forecast Accuracy for Ensembles of Distributed Stations Depending of the Size of the Region

The aim of the investigations in this section is to provide a model to estimate the forecast accuracy for arbitrary ensembles of stations and to investigate the forecast accuracy in dependence on the size of the region, where the stations are distributed.

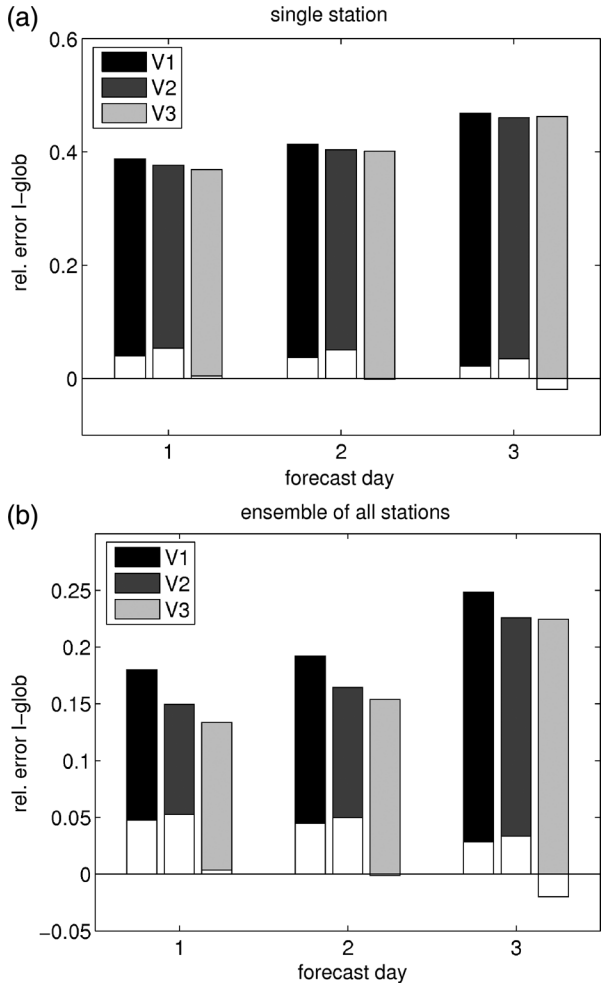

Fig. 6. Relative forecast errors for hourly global irradiance I_{glob} in dependence on the forecast horizon for the different forecasting approaches. (V1: linear interpolation of I_{glob}, V2: linear interpolation of kt^*, V3: linear interpolation of kt^* with clear sky model for clear sky situations and bias correction). Gray bars represent the *rRMSE*, the respective white bars show the *rBIAS*. (a) Single station. (b) Ensemble of all stations in Germany.

The reduction of errors when considering an ensemble of stations instead of a single station is determined by the cross correlation of forecast errors of the systems that are part of the ensemble. (see, e.g., [20]).

The cross correlation coefficient is defined as

$$r_{i,j}(t) = \frac{1}{N}\sum_{n=1}^{N} \varepsilon_i(t_n) \cdot \varepsilon_j(t_n) \tag{5}$$

where ε_i and ε_j, are bias corrected forecast errors normalized with respect to the standard deviation of forecast errors.

The correlation coefficient of the forecast errors of two stations depends on the distance between the stations, as illustrated in Fig. 7(a). This dependence can be modeled with an exponential function as proposed in [21]

$$r_{i,j}(d_{i,j}) = e^{(a_1 d_{i,j})^{a_2}} \tag{6}$$

where a_1 and a_2 are fit parameters and $d_{i,j}$ denotes the distance between the two stations. The light dots in Fig. 7(a) show the model curve.

Authorized licensed use limited to: Electricity Generating Authority of Thailand. Downloaded on August 23,2021 at 06:27:58 UTC from IEEE Xplore. Restrictions apply.

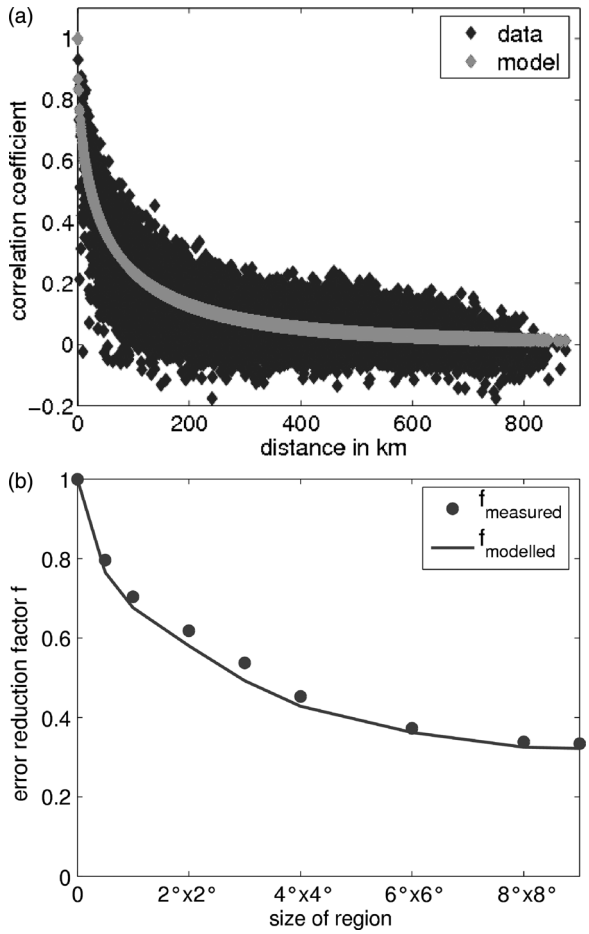

Fig. 7. (a) Correlation coefficient of forecast errors of two stations over the distance between the stations. The dark dots represent measured values; the light dots give the model curve. (b) Error reduction factor $\mathrm{RMSE}_{\mathrm{ensemble}}/\mathrm{RMSE}_{\mathrm{single}}$ for regions with increasing size.

This model in combination with a statistical approach to derive the expected errors of mean values allows for the estimation of the standard deviation of forecast errors $\mathrm{STDERR}_{\mathrm{ensemble}}$ for arbitrary scenarios of ensembles of stations ([20]). As the BIAS of the forecasts is very small (see Fig. 6), according to (4), the $\mathrm{RMSE}_{\mathrm{ensemble}}$ of an ensemble can be approximated by $\mathrm{STDERR}_{\mathrm{ensemble}}$ with good accuracy.

Fig. 7(b) shows the error reduction factor $f = \mathrm{RMSE}_{\mathrm{ensemble}}/\mathrm{RMSE}_{\mathrm{single}}$ calculated with this model for different ensembles of stations over the size of the region, where the stations are distributed. For comparison, the error reduction factor determined directly from the data is given. A good agreement between measured and modeled error reduction factors is achieved. For the present analysis all stations available within a region were used to determine the error reduction factor. Previous investigations in [22] have shown that already with a small number of sites a large reduction of the forecast errors is achieved. With increasing number of sites, the distance between the stations is decreasing. Hence, the correlation between the forecast errors of the single stations is increasing, as shown in Fig. 7(a). Consequently, the additional reduction of forecast errors when adding further sites to an ensemble is decreasing and saturation is reached for a certain number of stations, depending on the size of the region. For the results shown in Fig. 7(b) it can be assumed that this saturation level is reached and additional stations would not further reduce forecast uncertainty.

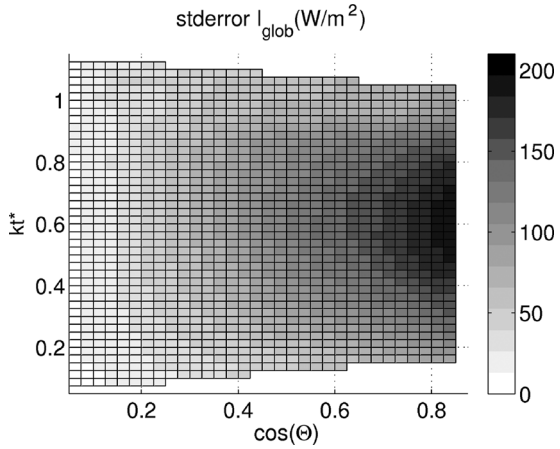

Fig. 8. STDERR of forecast of global irradiance I_{glob} in dependence on the cosine of the solar zenith angle $cos\Theta$ and the clear sky index kt^*.

Fig. 7(b) shows that for ensembles distributed over a region of a size of $3° \times 3°$, the RMSE of the forecast is about half the RMSE of a single site. The RMSE is reduced to one third of the site-specific RMSE for regions of a size of about $8° \times 8°$.

VI. Prediction Intervals

The specification of the forecast accuracy is an important issue for an effective application of the forecasts. Therefore, prediction intervals (see, e.g., [23]) are provided that indicate the range in which the actual value is expected to appear with a quantified probability. In order to model different accuracies of the forecast for different cloud situations, weather specific prediction intervals are determined on the basis of a detailed error analysis.

A. Method

For the calculation of prediction intervals, a model for distribution of forecast errors is necessary.

As a first approach, we assume a normal distribution of forecast errors with mean value zero for the different cloud and solar elevation situations. Accordingly, specific values of the STDERR are determined in dependence on the solar zenith angle and the cloud situation. In Fig. 8, the STDERR of the forecasts is displayed over the predicted clear sky index kt^* and the cosine of the solar zenith angle $cos\Theta$. The dependence of the STDERR on the two parameters can be modeled with a polynomial function of fourth order $stderr(cos\Theta, kt^*)$ with good accuracy. The fit parameters were derived on the training data set. Using this model, the expected STDERR can be estimated.

For mean values of ensembles of stations, the expected standard deviation of the forecast error is calculated as the product of the mean value of the modeled $stderr$ for the single stations and the error reduction factor f. The error reduction factor is calculated using the model proposed in Section V-C. Here, we

Authorized licensed use limited to: Electricity Generating Authority of Thailand. Downloaded on August 23,2021 at 06:27:58 UTC from IEEE Xplore. Restrictions apply.

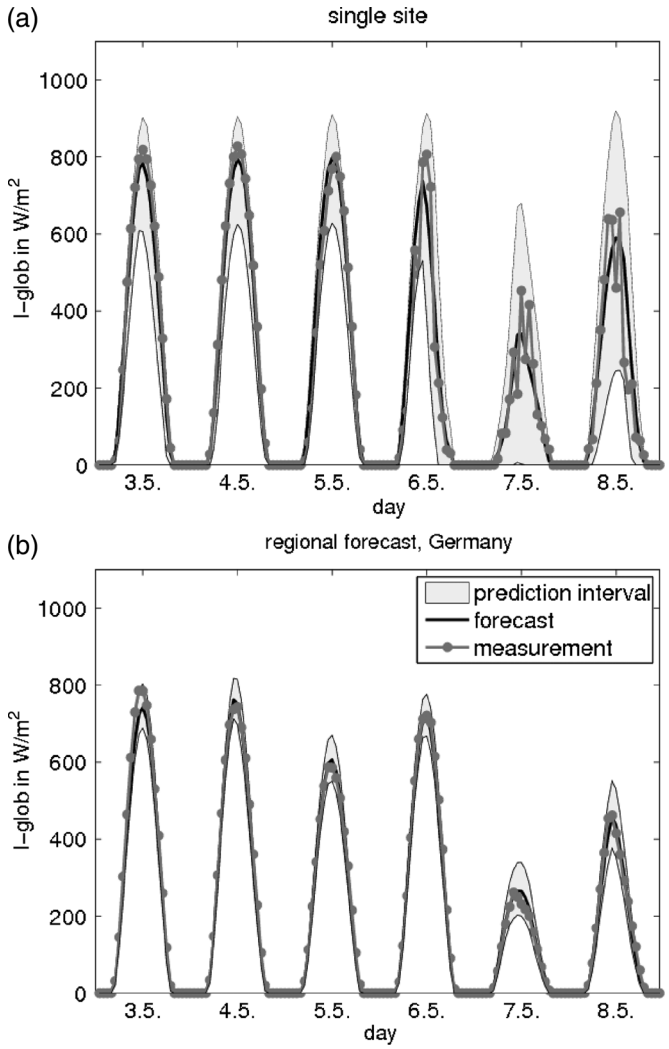

Fig. 9. Forecast of global irradiance I_{glob} with prediction intervals compared to measured irradiance for six days in May 2007 for a single site (a) and for the mean value of all measurement stations (b).

utilize again that STDERR and RMSE approximate each other with good accuracy, because the BIAS of the forecasts is small.

For a confidence level of 95% and using the assumption of a normal distribution, the upper limit of the prediction interval is given as

$$I_{\text{upper limit}} = I_{\text{forecast}} + 2^{*} stderr(cos\Theta, kt^{*}) \tag{7}$$

and the lower limit of the prediction intervals is calculated as

$$I_{\text{lower limit}} = I_{\text{forecast}} - 2^{*} stderr(cos\Theta, kt^{*}). \tag{8}$$

Additionally, these values are restricted to reasonable values between zero and maximum possible irradiance for a given solar zenith angle.

In Fig. 9, the forecasted irradiance values with prediction intervals of a confidence level of 95% are displayed in comparison to measured irradiance for six days in May 2007 for a single site [Fig. 9(a)] and for the mean value of the measurement stations distributed over Germany [Fig. 9(b)]. Fig. 9 illustrates that the changes of forecast quality with the meteorological situation are well modeled by the proposed approach. For clear sky situations, the prediction intervals are narrow, the forecast is very reliable. On days with variable clouds, large deviations are to be expected for forecasts with an hourly resolution for single stations or PV sites.

B. Evaluation

For a basic evaluation of the proposed procedure to derive prediction intervals, we determine the percentage of ground-measured values actually lying within the prediction intervals.

In addition

$$\Delta I_{\mathrm{rel}} = \sum_{i=1}^{N} (I_{\text{upper limit}} - I_{\text{lower limit}}) / \left(4 \sum_{i=1}^{N} I_{\mathrm{ground}} \right) \tag{9}$$

is given as a measure for the mean width of the prediction intervals. For a simple normal distribution this results in $\Delta I_{\mathrm{rel}} = r\mathrm{STDERR}$.

For single stations, 95% of all measured values are within the prediction intervals for the test set, the aimed reliability is achieved. The situation specific prediction intervals with $\Delta I_{\mathrm{rel}} = 28.4\%$ are in average considerably smaller than prediction intervals based on the assumption of a normal distribution with a constant STDERR.

For the evaluated ensemble of all stations, the prediction intervals with $\Delta I_{\mathrm{rel}} = 10.0\%$ are slightly too small. Only 91% of the measured values are found within the prediction intervals instead of the aimed 95%. A reason for this insufficiency might be that the error reduction factor f used to derive the prediction intervals for ensembles is assumed to be constant for all meteorological situations.

VII. Case Study: PV Power Forecast

The forecast of hourly global irradiance values as described in the last section provides the basis for the prediction of PV power output. This section gives a short overview on the models applied to derive the power forecast, followed by an evaluation of the forecast quality for a small ensemble of PV systems in a case study.

A. Models

The incoming irradiance is received on a tilted plane by most PV systems. Hence, the forecasted horizontal global irradiance has to be converted according to the orientation and declination of the modules for processing in the PV simulation model. Here, the anisotropic-all-sky model formulated by [24] is used.

In order to derive the power output forecast a robust simulation model for maximum power point (MPP) performance is applied to the forecasted irradiance on the tilted plane, together with models of the efficiency characteristics of the inverter and the different system losses (see [25]). The model returns the AC power fed to the grid as function of the incoming irradiance and the ambient temperature. Information on the ambient temperature here is included as measured values from nearby meteorological stations.

Authorized licensed use limited to: Electricity Generating Authority of Thailand. Downloaded on August 23,2021 at 06:27:58 UTC from IEEE Xplore. Restrictions apply.

B. Results

A detailed evaluation of the accuracy of PV power forecasts was performed in a case study for the ensemble of 11 PV systems shown in Fig. 2, based on irradiance forecasts with approach V2.

For single systems the evaluations resulted in an *rRSME* of 49% (absolute $\mathrm{RMSE} = 0.12$ Wh/Wp) for April, where cloudy situations were predominant. For July with mostly clear sky days for this region, a lower *rRMSE* of 30% (absolute $\mathrm{RMSE} = 0.10$ Wh/Wp) is found.

This analysis was complemented by the evaluation of predictions of irradiance on the tilted plane at the PV system sites, and an analysis of global horizontal irradiance forecasts for meteorological stations located in the same region. The errors of the PV power forecast are very closely related to the errors of the tilted irradiance forecast, and the RMSE values are similar. This holds only if the PV system parameters used for the simulation have a good quality, which was the case for the evaluated systems.

The quality of the global horizontal irradiance forecast with an *rRMSE* of 44% for April and an *rRMSE* of 28% for July is slightly better than the quality of the tilted irradiance and PV power forecast. Forecast errors are amplified by conversion of the irradiance on the tilted plane. However, given correct parameters to characterize the PV systems, the accuracy of the global horizontal irradiance forecast is still the determining factor for the quality of the power forecast.

The forecast errors are reduced to an *rRMSE* of 39% (absolute $\mathrm{RMSE} = 0.09$ Wh/Wp) for April and to an *rRMSE* of 22% (absolute $\mathrm{RMSE} = 0.06$ Wh/Wp) for July when considering the power production of the complete ensemble of 11 systems. This corresponds to an error reduction factor f of about 0.7 for the region of a size of 200 km $\times$ 120 km. Details of the evaluation are given in [26].

The proposed approach to derive prediction intervals for irradiance forecasts can be transferred to forecast of power output by applying error propagation according to [27]. The procedure proposed and validated in [27] additionally accounts for the uncertainty of the tilt conversion model and the PV system model. However, the STDERR of the power forecast, which is the basis to calculate respective prediction intervals, is mainly determined by the STDERR of the irradiance forecast.

VIII. Conclusions and Outlook

We have presented and compared several approaches to derive hourly site-specific irradiance forecasts from three-hourly ECMWF forecasts as a basis to predict PV power output. An optimum adjustment of the temporal resolution was achieved by combination with a clear sky model to consider the typical diurnal course of irradiance. Introducing an additional bias correction avoids systematic deviations for cloudy situations. The evaluation of hourly irradiance forecasts for single sites in Germany resulted in an overall *rRMSE* of 37% for the first forecast day, increasing to 46% for the third forecast day. An optimization of the proposed post processing procedure with respect to region and period for training and by consideration of additional parameters is currently under investigation.

Due to spatial averaging effects, the forecast for an ensemble of distributed systems shows higher accuracy than the forecast for single systems. The increase of the forecast accuracy essentially depends on the size of the region, where the PV systems are distributed. For a region of a size of $3^\circ \times 3^\circ$, the *rRMSE* of 19% is about half the *rRMSE* of a single site. The *rRMSE* is reduced to 13% for the complete German region with a size of $9^\circ \times 10^\circ$.

Furthermore, we have proposed and evaluated a first approach to derive weather specific prediction intervals. The derived prediction intervals provide a reasonable estimate for the expected maximum deviation of the measured from the predicted values for different meteorological situations. The proposed approach for prediction intervals will be further developed and transferred to PV power predictions.

The evaluation of PV power prediction in a case study has shown that the accuracy of the global horizontal irradiance forecast is the determining factor for the accuracy of the power forecast. For single PV systems, the RMSE of the hourly power prediction is in the range of 0.10 to 0.12 Wh/Wp. For the ensemble power prediction for a small region of 200 km$\times$ 120 km an RMSE in the range of 0.06 to 0.09 Wh/Wp was found. The analysis of PV power prediction will be extended to a large database of about 500 operating PV systems in Germany.

Acknowledgment

The authors would like to thank the European Centre for Medium-Range Weather Forecasts (ECMWF) for providing forecast data and Meteocontrol GmbH for supplying ground measurement data of solar irradiance and PV power output. The results of this paper are regarded as contribution to the IEA task "Solar Resource Knowledge Management"—a joint Task of the International Energy Agency's Implementing Agreements "Solar Heating & Cooling" (SHC), SolarPACES, and "Photovoltaic Power Systems" (PVPS).

References

[1] M. Lange, "A mature market? The history of short-term prediction services," presented at the POW'WOW Best-Practises Workshop, Delft, The Netherlands, 2006 [Online]. Available: http://www.powwow.risoe.dk/publ/ems-research_to_business_powwow_Delft_2006.pdf

[2] M. Lange and U. Focken, *Physical Approach to Short-Term Wind Power Prediction*. New York: Springer, 2005, 3-540-25662-8.

[3] A. Tindal, J. Parkes, L. Munoz, and J. Wasey, "Wind energy trading benefits through short term forecasting," presented at the European Wind Energy Conf., Athens, Greece, 2006 [Online]. Available: http://www.ewec2006proceedings.info/, 27.2-2.3

[4] D. Heinemann, E. Lorenz, and M. Girodo, "Forecasting of solar radiation," in *Solar Energy Resource Management for Electricity Generation From Local Level to Global Scale*, E. D. Dunlop, L. Wald, and M. Šúri, Eds. Hauppauge, NY: Nova, 2005.

[5] G. A. Grell, J. Dudhia, and D. R. Stauffer, A Description of the Fifth-Generation Penn State/NCAR Mesoscale Model (MM5), Tech. Note NCAR/TN-398+STR, National Center for Atmospheric Research. Boulder, CO, 1995.

[6] M. Girodo, "Solarstrahlungsvorhersage auf der Basis numerischer Wettermodelle," Ph.D. dissertation, Oldenburg Univ., Germany, 2006.

[7] R. J. Zamora, S. Solomon, E. G. Dutton, J. W. Bao, M. Trainer, R. W. Portmann, A. B. White, D. W. Nelson, and R. T. McNider, "Comparing MM5 radiative fluxes with observations gathered during the 1995 and 1999 Nashville southern oxidants studies," *J. Geophys. Res.*, vol. 108, pp. 1–13, 2003.

[8] R. Zamora, E. Dutton, M. Trainer, S. McKeen, J. Wilczak, and Y. Hou, "The accuracy of solar irradiance calculations used in mesoscale numerical weather prediction," *Monthly Weath. Rev.*, vol. 133, pp. 783–792, 2005.

Authorized licensed use limited to: Electricity Generating Authority of Thailand. Downloaded on August 23,2021 at 06:27:58 UTC from IEEE Xplore. Restrictions apply.

[9] R. A. Guarnieri, E. B. Pereira, and S. C. Chou, "Solar radiation forecast using artificial neural networks in South Brazil," in *Proc. 8 ICSHMO*, Foz do Iguaçu, Brazil, Apr. 24–28, 2006, pp. 1777–1785, INPE.
[10] R. Perez, K. Moore, and P. Stackhouse, "Forecasting solar radiation—Preliminary evaluation of an approach based upon the national forecast database," *Solar Energy*, vol. 81, no. 6, pp. 809–812, 2007.
[11] H. Breitkreuz, "Solare Strahlungsprognosen für energiewirtschaftliche Anwendungen—Der Einfluss von Aerosolen auf das sichtbare Strahlungsangebot," Ph.D. dissertation, Würzburg Univ., Germany, 2008.
[12] T. S. Nielsen, H. Madsen, H. A. Nielsen, P. Pinson, G. Kariniotakis, N. Siebert, I. Marti, M. Lange, U. Focken, L. von Bremen, P. Louka, G. Kallos, and G. Galanis, "Advanced statistical modelling and uncertainty assessment for wind power forecasting," presented at the European Wind Energy Conf., Athens, Greece, 2006 [Online]. Available: http://www.ewec2006proceedings.info/, 27.2-2.3
[13] P. Pinson, "Estimation of the Uncertainty in Wind Power Forecasting," Ph.D. dissertation, Ecole des Mines de Paris, Sophia Antipolis, France, 2006.
[14] I. T. Jolliffe and D. B. Stephenson, *Forecast Verification: A Practitioner's Guide in Atmospheric Science*. New York: Wiley, 2003.
[15] ECMWF-European Centre for Medium-Range Weather Forecasts, IFS Documentation Cy 31r1. IV. Physical Processes [Online]. Available: http://www.ecmwf.int/research/ifsdocs/CY31r1/index.html 2007
[16] J.-J. Morcette, "Radiation transfer, meteorological training course lecture series," in *Meteorological Training Course Lecture Series*. Reading, U.K.: ECMWF, 2000 [Online]. Available: http://www.ecmwf.int/newsevents/training/lecture_notes/LN_PA.html
[17] D. Dumortier, "Modelling global and diffuse horizontal irradiances under cloudless skies with different turbidities," Daylight II JOU2-CT92-0144, Final Report Vol. 2, 1995.
[18] B. Bourges, "Yearly variations of the Linke turbidity factor," in *Climatic Data Handbook of Europe*. Dordrecht, The Netherlands: Kluwer, 1992, pp. 61–64.
[19] D. Dumortier, The Satellight Model of Turbidity Variations in Europe, 1998, Tech. Rep.
[20] H. G. Beyer, "Space and Time Statistics of Wind and Solar Radiation Fields and Its Application to Renewable Energy System Analyses," Habilitation thesis, Univ. Oldenburg, Germany, 1994.
[21] S. Bofinger, H. G. Beyer, E. Lorenz, and H. Wikramarathne, "Validierung und Optimierung eines Solarstromprognosesystems unter Berücksichtigung von Ensemble-Effekten," presented at the 22. Symp. Photovoltaische Solarenergie, Bad Staffelstein, Germany, 2007, 6.3.-9.3.
[22] E. Lorenz, D. Heinemann, H. Wickramarathne, H. G. Beyer, and S. Bofinger, "Forecast of ensemble power production by grid-connected PV systems," presented at the 20th European PV Conf., Milano, Italy, 2007, 3.9-7.9.
[23] Hahn and Meeker, *Statistical Intervals—A Guide for Practitioners*. New York: Wiley, 1991.
[24] T. M. Klucher, "Evaluation of models to predict insolation on tilted surfaces," *Solar Energy*, vol. 23, pp. 111–114, 1979.
[25] A. Drews, H. G. Beyer, and U. Rindelhardt, "Quality of performance assessment of PV plants based on irradiance maps," *Solar Energy*, 2007, 10.1016/j.solener.2008.04.009, submitted for publication.
[26] H. Wickramarathne, "Evaluation of Forecast of Power Production With Distributed PV-Systems," M.S. thesis, Postgraduate Programme Renewable Energy, Oldenburg Univ., Germany, 2007.
[27] E. Lorenz, "Intelligent Performance Check of PV System Operation Based on Satellite Data," PVSAT-2, ENK5-CT2002-00631, Final Rep., 2007.

Elke Lorenz, photograph and biography not available at the time of publication.

Johannes Hurka, photograph and biography not available at the time of publication.

Detlev Heinemann, photograph and biography not available at the time of publication.

Hans Georg Beyer, photograph and biography not available at the time of publication.

Authorized licensed use limited to: Electricity Generating Authority of Thailand. Downloaded on August 23,2021 at 06:27:58 UTC from IEEE Xplore. Restrictions apply.